

Towards Efficient SDRTV-to-HDRTV by Learning from Image Formation

Xiangyu Chen*, Zheyuan Li*, Zhengwen Zhang, Jimmy S. Ren, Yihao Liu, Jingwen He, Yu Qiao, *Senior Member, IEEE*, Jiantao Zhou, *Senior Member, IEEE*, Chao Dong

Abstract—Modern displays are capable of rendering video content with high dynamic range (HDR) and wide color gamut (WCG). However, the majority of available resources are still in standard dynamic range (SDR). As a result, there is significant value in transforming existing SDR content into the HDRTV standard. In this paper, we define and analyze the SDRTV-to-HDRTV task by modeling the formation of SDRTV/HDRTV content. Our analysis and observations indicate that a naive end-to-end supervised training pipeline suffers from severe gamut transition errors. To address this issue, we propose a novel three-step solution pipeline called HDRTVNet++, which includes adaptive global color mapping, local enhancement, and highlight refinement. The adaptive global color mapping step uses global statistics as guidance to perform image-adaptive color mapping. A local enhancement network is then deployed to enhance local details. Finally, we combine the two sub-networks above as a generator and achieve highlight consistency through GAN-based joint training. Our method is primarily designed for ultra-high-definition TV content and is therefore effective and lightweight for processing 4K resolution images. We also construct a dataset using HDR videos in the HDR10 standard, named HDRTV1K that contains 1235 and 117 training images and 117 testing images, all in 4K resolution. Besides, we select five metrics to evaluate the results of SDRTV-to-HDRTV algorithms. Our final results demonstrate state-of-the-art performance both quantitatively and visually. The code, model and dataset are available at <https://github.com/xiaom233/HDRTVNet-plus>.

Index Terms—Image processing, Image Enhancement, Gamut extension.

1 INTRODUCTION

THE resolution of television (TV) and film content has updated from standard definition (SD) to full high definition (FHD) and, most recently, to ultra-high definition (UHD). High dynamic range is one of the most promising features of the UHD TV definition. HDRTV¹ content has much wider color gamut and a higher dynamic range than SDRTV content, so HDRTV standard allows us to enjoy images and videos that are closer to what we see in real life. While HDR display devices have become prevalent in daily life, most accessible resources are still in SDRTV format. Therefore, algorithms are needed to convert SDRTV content to their HDRTV version. The task, denoted as SDRTV-to-HDRTV, is of great practical value but has received less attention in the research community. The reason is mainly twofold. First, existing HDRTV standards (e.g., HDR10 and HLG) have not been well-defined until recent years. Second, there is a lack of large-scale datasets for training and testing. To promote the development of this emerging area, we conduct in-depth research on the SDRTV-to-HDRTV problem in this paper.

SDRTV-to-HDRTV is a very challenging problem due to

- Xiangyu Chen and Jiantao Zhou are with State Key Laboratory of Internet of Things for Smart City, University of Macau.
- Xiangyu Chen, Zheyuan Li, Zhengwen Zhang, Yihao Liu, Chao Dong and Yu Qiao are with Shenzhen Institutes of Advanced Technology, Chinese Academy of Sciences, Shenzhen, China.
- Xiangyu Chen, Yihao Liu, Jingwen He, Chao Dong and Yu Qiao are with Shanghai Artificial Intelligence Laboratory, Shanghai, China.
- Jimmy S. Ren is with SenseTime Research, Hong Kong, China.

Co-first Authors: Xiangyu Chen and Zheyuan Li; Corresponding Authors: Chao Dong (chao.dong@siat.ac.cn) and Jiantao Zhou (jtzhou@um.edu.mo).

1. We add a suffix TV after HDR/SDR to indicate content under the HDRTV/SDRTV format and standard.

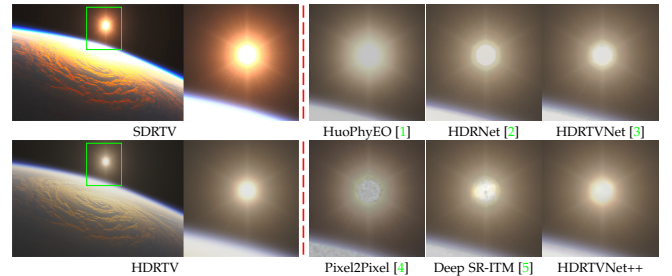


Fig. 1. The visual comparison of different methods to deal with the SDRTV-to-HDRTV task.

the differences in dynamic range, color gamuts, and bit-depths between the two types of content. Essentially, both SDRTV and HDRTV content are derived from the same raw file, while they are processed under different standards. It is important to note that the SDRTV-to-HDRTV task differs from the LDR-to-HDR task, despite the similar naming, as it involves entirely different considerations. Specifically, LDR-to-HDR methods [1], [6], [7], [8], [9] aim to predict the HDR scene luminance in the linear domain, which is actually closer to the Raw file. A classic LDR formation pipeline mentioned in recent work SingleHDR [8]. In order to better understand the concepts of SDRTV/HDRTV and the task of SDRTV-to-HDRTV, we provide more detailed explanations in Section 2. From the perspective of the imaging formation process, SDRTV-to-HDRTV can be viewed as an image-to-image translation task [4], [10]. Due to the significant difference in color gamut between SDRTV and HDRTV content, photo retouching methods [2], [11], [12] can be employed to deal with the SDRTV-to-HDRTV task and handle the color

transformation. While not exclusively dedicated to SDRTV-to-HDRTV, Deep SR-ITM [5] and JSI-GAN [13] are among the earliest works in the computer vision community to address this task by jointly solving super-resolution and SDRTV-to-HDRTV. We provide an illustration of SDRTV-to-HDRTV and visual comparison results of different kinds of methods in Figure 1. As can be seen, all previous methods have difficulty handling this problem effectively.

This paper aims to address SDRTV-to-HDRTV through a deep understanding of this underlying issue. We first introduce a simplified formation pipeline for SDRTV/HDRTV content, consisting of tone mapping, gamut mapping, transfer function and quantization. Based on the formation pipeline, we propose our method HDRTVNet++, whose solution pipeline consists of three parts: adaptive global color mapping (AGCM), local enhancement (LE) and highlight refinement (HR). Specifically, AGCM employs a novel color condition block to extract global image priors and adapt to different images. It uses only 1×1 filters to achieve superior performance with fewer parameters compared to other photo retouching methods such as CSRNet [14], HDRNet [2] and Ada-3DLUT [12]. Following AGCM, we design a U-shape network with spatial conditions as the LE network, to achieve local enhancement that AGCM cannot handle. We find that processing color mapping first and then performing local enhancement can effectively avoid color transition artifacts produced by directly training an end-to-end network. This is likely due to the difficulty for convolutional networks to simultaneously learn global color transformation and high-frequency detail enhancement. After training the AGCM and LE networks, joint finetuning can further improve the SDRTV-to-HDRTV results. Although AGCM and LE have been able to achieve good results, we find that the visual quality of the highlight areas is still not satisfactory. Due to the severe information loss caused by color gamut truncation and dynamic range truncation in these areas, it is difficult for an MSE-based method to achieve good results. Therefore, we adopt generative adversarial training as the highlight refinement part to further enhance the visual results in highlight regions.

To advance research in this new area, we construct a new large-scale dataset called HDRTV1K. We also select five evaluation metrics – PSNR, SSIM, SR-SIM [15], ΔE_{ITP} [16] and HDR-VDP3 [17] to assess mapping accuracy, structural similarity and color accuracy.

In summary, our contributions are four-fold:

- We conduct a detailed analysis of the SDRTV-to-HDRTV task by modeling the formation of SDRTV/HDRTV content.
- We propose an efficient SDRTV-to-HDRTV method that achieves the state-of-the-art performance both quantitatively and qualitatively.
- We present a global color mapping network based on color condition blocks, which achieves outstanding color mapping accuracy with only 35K parameters.
- We provide an HDRTV dataset and select five metrics to evaluate SDRTV-to-HDRTV algorithms.

A preliminary version of this work was presented at ICCV2021 [3]. Following the proposed settings of SDRTV-to-HDRTV, several works have investigated this problem

[18], [19], [20], [21], [22]. The present work significantly improves upon the initial version in several ways. Firstly, we improve upon our initial method, HDRTVNet, by proposing HDRTVNet++ with a better pipeline design and more effective network. Specifically, we jointly train AGCM and LE to achieve better restoration accuracy. We then remove the heavy sub-network of highlight generation and use a joint adversarial training strategy instead. Compared with HDRTVNet, the improved method HDRTVNet++ achieves a significant performance gain of 0.99dB on PSNR with much fewer parameters. Secondly, we provide more detailed explanations and analysis of the motivation and rationality behind our proposed solution pipeline. By formulating pixel-independent and region-dependent operations, we emphasize the importance of the correct order of global color mapping and local enhancement. Besides, we present additional experimental analysis to illustrate this crucial point for SDRTV-to-HDRTV. Thirdly, we conduct more extensive experiments for ablation study and investigations more details for the network design. Through these experiments, we further demonstrate the effectiveness of our proposed modules and the overall method.

2 PRELIMINARY

In this section, we clarify the concept of SDRTV/HDRTV and the meaning of SDRTV-to-HDRTV and LDR-to-HDR, since these terms are often easily confused and few previous works address this issue.

Concept. In this paper, we use SDRTV/HDRTV to represent the content (including image and video) under SDRTV/HDRTV standards. The two standards are specified in [23], [24] and [25], [26], respectively. The basic elements of the HDRTV standard mainly include wide color gamut [25], PQ or HLG OETF [26], and 10-16 bits depth. Content that does not conform to the HDRTV standard is generally considered to be SDR, while the SDRTV standard defines the content requirements more clearly (e.g., Rec.709 color gamut and gamma-OETF). The same content can be encoded using these two standards, while the amount of information that can be accommodated by each standard differs. This difference in capacity results in varying visual experiences for the two types of content. For the terminology of LDR/SDR, Both terms can refer to low dynamic range content; however, there are some differences in their usage. Specifically, SDR often refers to display devices and related standards, which is commonly used in content production or post-production processing. Therefore, SDR content is typically video or frames under the SDR standard, derived from high dynamic range RAW files. In contrast, LDR content is often images or multiple frames captured by a camera at a specific exposure level. As a result, its dynamic range is determined during the imaging stage. In simple terms, there are some differences in the formation process between the two types of content. We emphasize that neither of the two concepts has a strict academic definition. For clarity, we use the terms **LDR-to-HDR** and **SDRTV-to-HDRTV** to represent the conventional image HDR reconstruction and the up-conversion of content from SDRTV to HDRTV standard.

Explanation. We explain that SDRTV-to-HDRTV is functionally different from the previous LDR-to-HDR (i.e., in-

verse tone mapping) problem. Although both involve the concept of HDR, the connotations of HDR are not the same in these two issues. There are overwhelming amount of data-level details for the differences of these two things. In general, LDR-to-HDR methods aim to predict the luminance of images in the linear domain, representing the physical brightness of a scene. HDR here refers to high dynamic range information that cannot be captured by low dynamic range imaging. In contrast, SDRTV-to-HDRTV is to predict HDR images in the pixel domain using the HDR *display format* encoded in HDRTV standards, such as HDR10, HLG and Dolby Vision. Content in the HDRTV standard comes from the same source as content in the SDRTV standard, both derived from HDR scene radiance. HDRTV content can also be produced from linear domain HDR content, but this process requires additional engineering operations, such as tone mapping and gamut mapping. As a result, methods for these two different tasks are not interchangeable.

3 RELATED WORK

3.1 SDRTV-to-HDRTV

The task of SDRTV-to-HDRTV task, which is the focus of this paper, is first mentioned in [27]. In that paper, the task was referred to as inverse tone mapping (ITM) and SDRTV/HDRTV content mentioned in this paper is represented as LDR/HDR. Deep SR-ITM [5] and JSI-GAN [13] have demonstrated impressive results in jointly training image super-resolution and SDRTV-to-HDRTV conversion, attracting much attention from researchers to the task of SDRTV-to-HDRTV. The conference version of this work, HDRTVNet [3] firstly delves into this problem, proposing a detailed analysis, a basic solution and a dataset. Following [3], several works have been proposed to address the task of SDRTV-to-HDRTV. For example, He *et al.* [19] proposes HD-CFM, which introduces hierarchical global and local feature modulation to deal with this task. To enhance the contrast in a frequency-adaptive way for SDRTV-to-HDRTV conversion, Xu *et al.* [18] introduces a Frequency-aware Modulation Network (FMNet) that reduces the structural distortions and artifacts. Cheng *et al.* [20] proposes a learning-based SDR data synthesis approach to synthesize realistic SDRTV-HDRTV pairs for better generalization of SDRTV-to-HDRTV methods. Guo *et al.* [22] provides a new dataset and degradation models for practical SDRTV-to-HDRTV conversion. In this work, we further improve the conference version [3] by proposing more effective and efficient networks with more analysis and experiments.

3.2 Gamut Extension

Gamut extension, a widely recognized concept in color science, involves converting image or video content to a wider color gamut. A crucial step in the SDRTV-to-HDRTV process is converting the color gamut from Rec.709 to Rec.2020. As a result, gamut extension algorithms can be used to address the SDRTV-to-HDRTV task in certain situations. ITR [28] provides a recommended color conversion matrix for gamut extension. However, it does not consider color mappings (e.g. tone mapping) used in actual production, making it unsuitable for addressing SDRTV-to-HDRTV conversion.

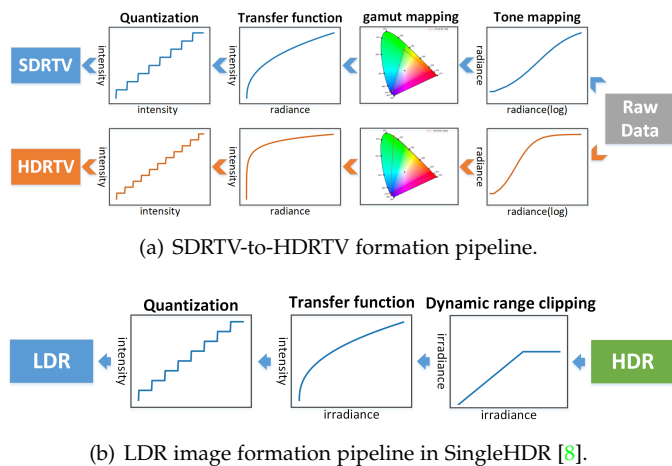


Fig. 2. Analysis of SDRTV-to-HDRTV and LDR-to-HDR formations.

Many gamut extension algorithms have been proposed in recent years [29], [30], [31], [32], [33], [34]. For instance, [29] introduces a perceptually-based variational framework for spatial gamut mapping. [34] presents a PDE-based optimization procedure that considers the hue, chroma, and saturation for gamut extension. [34] proposes a vision science-based framework for performing gamut extension. However, these algorithms are primarily designed for color mapping in SDRTV-to-HDRTV and are not capable of handling more complex operations for detail enhancement.

4 ANALYSIS

In this section, we present a streamlined SDRTV/HDRTV formation pipeline that contains the most critical steps in actual production. Subsequently, we analyze the formation pipeline and propose a new solution based on the idea of divide-and-conquer.

4.1 SDRTV/HDRTV Formation Pipeline

We introduce a simplified formation pipeline of SDRTV and HDRTV based on camera ISP and HDRTV content production [35] as depicted in Figure 2(a). While some operations, such as denoising, white balance in camera pipeline, and color grading in HDR content production are not discussed, we retain the four key operations that lead to the primary differences between SDRTV and HDRTV: tone mapping, gamut mapping, opto-electronic transfer function and quantization. In the subsequent equations, we use “S” to represent SDRTV and “H” to represent HDRTV.

Tone mapping. Tone mapping is used to transform the high dynamic range signals into low dynamic range signals to accommodate different display devices. This process includes global tone mapping [36], [37], [38] and local tone mapping [39], [40]. Global tone mapping applies the same function to all pixels, with parameters generally related to global image statistics (e.g., average luminance). Local tone mapping can adapt to local content and human preferences but often incurs high computational costs and artifacts. As a result, global tone mapping is primarily used in

SDRTV/HDRTV image formation. The function of global tone mapping can be expressed as follows:

$$I_{tS} = T_S(I|\theta_S), I_{tH} = T_H(I|\theta_H), \quad (1)$$

where T_S and T_H represent the specific tone mapping functions, θ_S and θ_H are coefficients related to image statistics. It is noteworthy that S-shape curves are commonly used for global tone mapping and clipping operations often occur during the actual process of tone mapping. For example, curves of Hable tone mapping [41] for SDRTV (0 - 100cd/m²) and HDRTV (0 - 10000cd/m²) are depicted in Figure 2(a).

Gamut mapping. Gamut mapping is to convert colors from the source gamut to the target gamut while preserving the overall appearance of the scene. According to ITU-R standards [23] and [25], the transformations from the original XYZ space to SDRTV (Rec.709) and HDRTV (Rec.2020) can be represented as:

$$\begin{bmatrix} R_{709} \\ G_{709} \\ B_{709} \end{bmatrix} = M_S \begin{bmatrix} X \\ Y \\ Z \end{bmatrix}, \begin{bmatrix} R_{2020} \\ G_{2020} \\ B_{2020} \end{bmatrix} = M_H \begin{bmatrix} X \\ Y \\ Z \end{bmatrix}, \quad (2)$$

where M_S and M_H are constant 3×3 matrices. As illustrated in Figure 2(a), we use the CIE chromaticity diagram to differentiate between the target gamuts of SDRTV and HDRTV, which correspond to Rec.709 and Rec.2020, respectively.

Opto-electronic transfer function. The opto-electronic transfer function (OETF) converts linear optical signals into non-linear electronic signals in the image formation pipeline. For SDRTV, it approximates a gamma exponential function as $I_{fS} = f_S(I) = I^{1/2.2}$. For HDRTV, several OETFs exist for different standards, such as PQ-OETF [42] for the HDR10 standard and HLG-OETF [26] for the HLG standard (HLG stands for Hybrid Log-Gamma). As an example, we consider the PQ-OETF:

$$I_{fH} = f_H(I) = \left(\frac{a_1 + a_2 I^{b_1}}{1 + a_3 I^{b_1}} \right)^{b_2}, \quad (3)$$

where a_1, a_2, a_3, b_1, b_2 are constants. The curves of gamma-OETF for SDRTV (0 - 100cd/m²) and PQ-OETF for HDRTV (0 - 10000cd/m²) are depicted in Figure 2(a).

Quantization. After the aforementioned operations, the encoded pixel values are quantized using the function:

$$I_q = Q(I, n) = \frac{[(2^n - 1) \times I + 0.5]}{2^n - 1}, \quad (4)$$

where n is 8 for SDRTV and 10-16 for HDRTV.

In summary, the SDRTV and HDRTV content formation pipelines can be expressed as:

$$I_S = Q_S \circ f_S \circ M_S \circ T_S(I_{raw}), \quad (5)$$

$$I_H = Q_H \circ f_H \circ M_H \circ T_H(I_{raw}), \quad (6)$$

where \circ denotes the connection between two operations.

Comparison with LDR formation pipeline. In Single-HDR [8], the LDR image formation pipeline is simplified as in Figure 2(b). The camera pipeline for HDR-to-LDR comprises three main parts: dynamic range clipping, non-linear mapping (i.e., applying a transfer function), and quantization. In this pipeline, "HDR" represents the scene radiance, while color mapping is not involved. Similarly, for

SDRTV/HDRTV formation, the process also contains dynamic range compression, transfer function application and quantization. However, there are two essential differences between the LDR formation pipeline and SDRTV/HDRTV pipeline. First, for LDR-to-HDR, the LDR image is generated from HDR scene radiance, making LDR-to-HDR a kind of reverse process to some extent. In contrast, SDRTV and HDRTV are generated from the same raw data (or resource in Log format) using different operations for different standards as depicted in Eqs. (5) and (6). Second, color conversion is generally not involved in LDR-to-HDR, as "HDR" has been converted from camera RGB to sRGB, which is typically encoded in the same color gamut as LDR. However, gamut extension is a crucial step in SDRTV-to-HDRTV. Overall, we present the formation pipeline to illustrate the key production steps that lead to the differences between SDRTV and HDRTV content.

4.2 SDRTV-to-HDRTV Solution Pipeline

According to the above formation pipeline, the SDRTV-to-HDRTV process can be formulated as:

$$I_H = Q_H \circ f_H \circ M_H \circ T_H \circ T_S^{-1} \circ M_S^{-1} \circ f_S^{-1} \circ Q_S^{-1}(I_S), \quad (7)$$

where $T_S^{-1}, M_S^{-1}, f_S^{-1}, Q_S^{-1}$ represent the inversion of the corresponding operations. Instead of adopting an end-to-end solution, we propose a new solution pipeline, (as shown in Figure 3(a)), based on the following observations. First, many critical operations in the formation pipeline are pixel-independent operations (i.e., the manipulation on one pixel is uncorrelated with its neighboring pixels), such as global tone mapping, OETF, and gamut mapping. Furthermore, the inversion of these operations is also pixel-independent. Second, some operations, such as local tone mapping and dequantization, rely on information from a region to reconstruct the results. We refer to these as region-dependent operations.

To better understand these two types of operations, we formulate the mapping $f(\cdot)$ from the input I_{in} to the output I_{out} located at (x, y) as:

$$I_{out}(x, y) = f(\Omega(I_{in}(x, y), \delta)), \quad (8)$$

where $\Omega(I_{in}(x, y), \delta)$ denotes a local region in I_{in} . It composed of pixels whose distance from the center point $I_{in}(x, y)$ is no more than δ . Specially, $\delta = 1$ means that $\Omega(I_{in}(x, y), \delta)$ is equivalent to $I_{in}(x, y)$. Thus, pixel-independent operations can be expressed as:

$$I_{out}(x, y) = f(\Omega(I_{in}(x, y), 1)) = f(I_{in}(x, y)), \quad (9)$$

while the region-dependent operations are formulated as:

$$I_{out}(x, y) = f(\Omega(I_{in}(x, y), \delta)), \text{ where } \delta > 1. \quad (10)$$

As color conversion is a crucial part of actual production for SDRTV-to-HDRTV [28], we implement pixel-independent and region-dependent operations separately, i.e., global color mapping and local enhancement in Figure 3(a). Given that the global color mapping is typically related to the image content (e.g., the average brightness and peak brightness of the content may affect the tone mapping

curve), we believe that global color mapping should have the image-adaptive property as:

$$I_{out}(x, y) = f(I_{in}(x, y)|I_{in}). \quad (11)$$

Experiments in Section 6.2 demonstrate the effectiveness and efficiency of our design. Additionally, we find that performing the pixel-independent operation first and then processing the region-independent operation significantly reduces the color transition artifacts brought by the end-to-end solution, as shown in Figure 8. We speculate that this is due to the optimization difficulty for convolution operators to simultaneously process pixel-independent low-frequency color transformation and region-dependent high-frequency transformation. For better performance, we further optimize the two operations jointly.

Moreover, there is severe information compression/loss for SDRTV content, particularly in highlight areas. This is due to the clipping operations on dynamic range and color gamut in the image formation. The previous version [3] attempts to predict the missing information through additional highlight generation network, but the results are unsatisfactory. The large area of information loss in the over-saturated regions is too difficult to recover. Nevertheless, we find that generative adversarial training can enhance the visual quality of predictions by improving color transitions in highlight areas. It is because that the generative adversarial training can make the prediction close to the distribution of HDRTV content.

We compare different SDRTV-to-HDRTV solution pipelines in Figure 3. Existing learning-based SDRTV-to-HDRTV methods [5], [13], [18] directly learn end-to-end networks, as shown in Figure 3(b). Since LDR-to-HDR has been extensively discussed, we also demonstrate how to achieve SDRTV-to-HDRTV based on the LDR-to-HDR method in principle. As depicted in Figure 3(c), the HDR radiance map is first generated using the LDR-to-HDR method. Then, gamut mapping is applied to convert the radiance map to the Rec.2020 gamut. The PQ OETF is subsequently used to compress the dynamic range. Finally, quantization is performed to produce the HDRTV output. We emphasize that the details of these operations may vary in actual processing, and we follow the pipeline used in [5], [13]. In contrast, our solution pipeline addresses the problem step by step using a divide-and-conquer strategy.

5 METHODOLOGY

Based on the proposed solution pipeline, we develop a new method called HDRTVNet++, which consists of three steps: adaptive global color mapping, local enhancement and highlight refinement. In this section, we provide a detailed description of each component in the method.

5.1 Adaptive Global Color Mapping

Adaptive global color mapping (AGCM) aims to achieve image-adaptive color mapping from the SDRTV domain to the HDRTV domain. In this paper, we adopt the same network structure for AGCM as the initial version, but improve the training. As shown in Figure 4, the proposed model comprises a base network and a condition network.

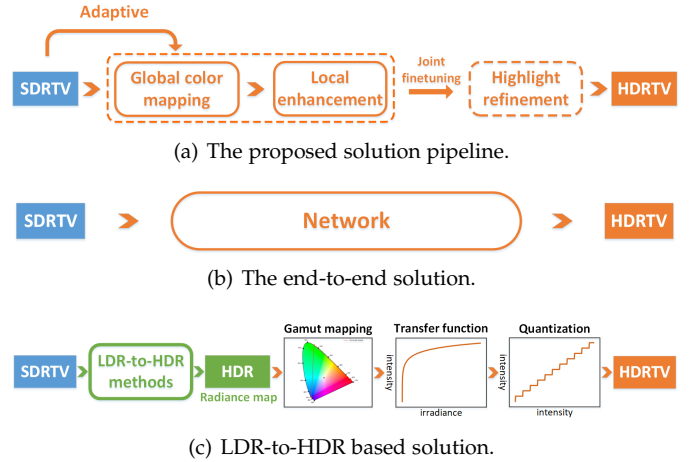


Fig. 3. SDRTV-to-HDRTV solution pipelines.

5.1.1 Base Network

The base network is designed to handle pixel-independent operations. Let I_S be the input SDRTV image. This mapping can be denoted as:

$$I_B(x, y) = f(I_S(x, y)), \forall (x, y) \in I_S, \quad (12)$$

where (x, y) represents the coordinate of the pixel in the image I , and I_B represents the output of base network. As demonstrated in CSRNet [11], a fully convolutional network with only 1×1 convolutions and activation functions can achieve pixel-independent mapping. Thus, our base network is composed of N_l convolutional layers with 1×1 filters and N_l-1 ReLU activation functions, which can be denoted as:

$$I_B = Conv_{1 \times 1} \circ (ReLU \circ Conv_{1 \times 1})^{N_l-1}(I_S). \quad (13)$$

The proposed base network takes an 8-bit SDRTV image as input and generates an HDRTV image encoded with 10-16 bits. Although the base network can only learn a one-to-one color mapping, it still achieves considerable performance, as shown in Table 1. It is worth noting that the base network can perform like a 3D lookup table (3D LUT), but with fewer parameters. Experiments with quantitative comparisons are shown in Section 6.7.

5.1.2 Condition Network

Global priors are essential for adaptive global color mapping. For example, global tone mapping requires global image statistics like maximum brightness and average brightness. To achieve image-adaptive mapping, we add a condition network to modulate the base network. Previous works [14], [43], [44] typically adopt image content prior, where the condition network extracts spatial and local information from the input image by $N_k \times N_k$ ($N_k > 1$) filters. However, for the SDRTV-to-HDRTV problem, global mapping is mostly conditioned on global image statistics or color distribution. This type of color condition is independent of spatial information, so it may not be suitable for previous condition structures to deal with this problem. Our proposed condition network focuses on extracting color-related information to achieve adjustable mapping. As illustrated

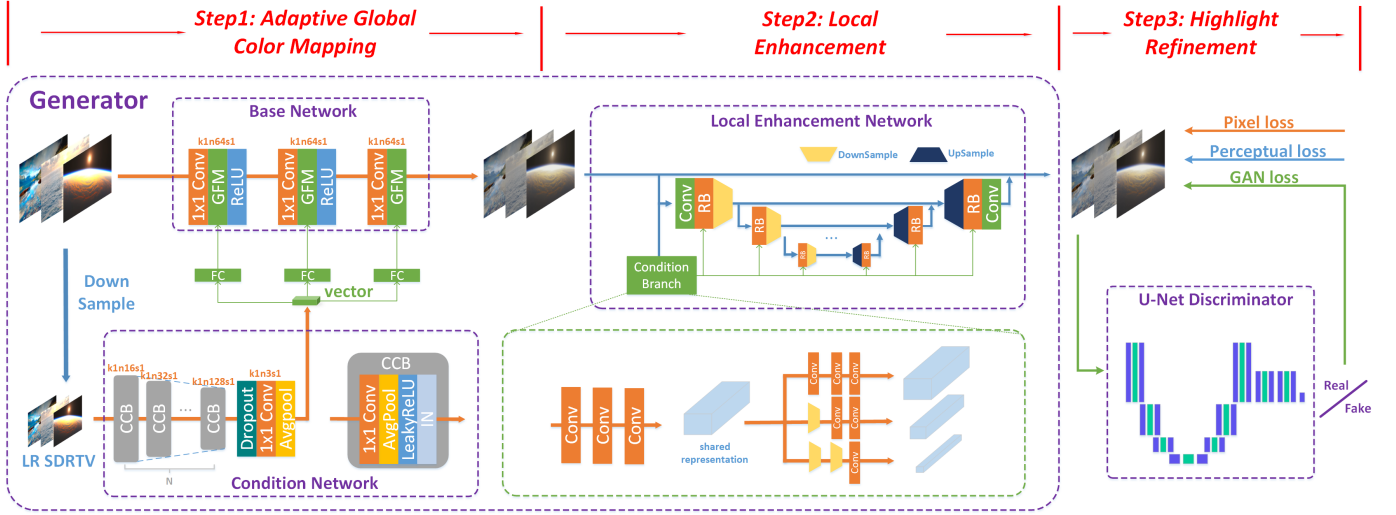


Fig. 4. The architecture of the proposed SDRTV-to-HDRTV method.

in Figure 4, the condition network consists of several color condition blocks, convolution layers, feature dropout and global average pooling.

Color condition block. A color condition block (CCB) contains a convolution layer with 1×1 filters, an average pooling operation, a LeakyReLU activation, and an instance normalization layer [45], which can be written as:

$$CCB(I_f) = IN \circ LReLU \circ avgpool \circ Conv_{1 \times 1}(I_f), \quad (14)$$

where I_f denotes the input features of CCB. The condition network takes a down-sampled SDRTV image as input and outputs a condition vector V . The condition network is formulated as:

$$V = GAP \circ Conv_{1 \times 1} \circ Dropout \circ CCB^{N_c}(I_S). \quad (15)$$

Since the convolutional layers only contain 1×1 filters, the condition network does not extract local features. With the help of pooling layers, the network can extract global priors based on image statistics. To avoid overfitting, we add a dropout layer before the last convolutional layer and global average pooling. This performs like adding a multiplicative Bernoulli noise to features.

5.1.3 Global Feature Modulation

To utilize the extracted global priors, we introduce the global feature modulation (GFM) [14] mechanism, which has been successfully applied in photo retouching tasks. Through GFM, the intermediate features of the base network can be modulated by scaling and shifting operations according to the condition vector. It can be described as:

$$GFM(x_i) = \alpha * x_i + \beta, \quad (16)$$

where x_i denotes the feature map to be modulated. α and β represent the scale and shift factor, respectively.

Overall, the AGCM network can be formulated as:

$$I_{AGCM} = GFM \circ Conv_{1 \times 1} \circ (ReLU \circ GFM \circ Conv_{1 \times 1})^{N_i-1}(I_S), \quad (17)$$

where I_{AGCM} denotes the output of adaptive global color mapping. To optimize adaptive global color mapping, we minimize the distance between the output and the ground-truth HDRTV image using the L1 loss function.

5.2 Local Enhancement

Although AGCM can obtain considerable performance, local enhancement is essential for SDRTV-to-HDRTV. For a specific image, AGCM can still only perform one-to-one color mapping. In order to continue expanding the color gamut and handle some potential local mappings, region-dependent local operators are also necessary. In the preliminary version [3], we simply adopt a classic ResNet to achieve local enhancement. Despite its simplicity, this design imposes limitations on SDRTV-to-HDRTV performance and introduces a significant computational burden. In this paper, we draw inspiration from [44] and employ a UNet structure for local enhancement.

Specifically, the local enhancement network contains a main branch and a condition branch, as presented in Figure 4. The main branch is a U-shape structure and the condition branch generates the condition vector to modulate the intermediate features of the main branch. We take the output of AGCM $I_{AGCM} \in \mathbb{R}^{3 \times H \times W}$ as input for the local enhancement network. In the main branch, the input is first mapped to a high-dimensional feature $F_0 \in \mathbb{R}^{C \times H \times W}$, where C is the number of channels. Subsequently, the shallow feature F_0 is processed through a three-level symmetric encoder-decoder to refine the features. Within the encoder, the spatial size of the feature is progressively reduced while the number of blocks is gradually increased from the top to bottom levels. The decoder takes low-resolution latent features as input and reconstructs the high-resolution representation. For downsampling and upsampling in the U-shape structure, we use stride convolution and pixel-shuffle operations [46], respectively. To assist the recovery process, skip connections are introduced for encoder features and decoder features. In real-world scenarios, SDRTV content is typically in the range of 1K to 4K resolution. The use of a U-shape structure can significantly reduce the computational

burden required for processing. For the condition branch, we first use three convolutions to process the input for a shared representation. Then, hierarchical conditions are generated to modulate the intermediate features of the main branch. In the part of local enhancement, we aim to implement the region-dependent operation and further address the spatially variant mapping for SDRTV-to-HDRTV. Thus, we employ the SFT layer [43] and leverage its ability of spatial feature modulation to build the network. The SFT layer is denoted as:

$$SFT(x_i) = m \odot x_i + n, \quad (18)$$

where \odot denotes the element-wise multiplication. $x_i \in \mathbb{R}^{C \times H \times W}$ is the intermediate features to be modulated. $m \in \mathbb{R}^{C \times H \times W}$ and $n \in \mathbb{R}^{C \times H \times W}$ are two condition maps predicted by the condition branch. It is important to note that when local enhancement networks (i.e., region-dependent operations), are used to learn end-to-end mapping without the inclusion of adaptive global color mapping, the resulting output often exhibits noticeable artifacts. This is illustrated in Figure 8. To achieve better optimization, we further jointly train the AGCM and LE networks. Experiments show that joint training can still bring a slight performance improvement. Benefiting from our AGCM and LE, the proposed method can significantly outperform existing approaches with high efficiency for SDRTV-to-HDRTV.

5.3 Highlight Refinement

Our solution pipeline includes a crucial step called highlight refinement (HR), which aims to solve the color inconsistency in highlight regions caused by extreme compression and clipping. Due to the high degree of ill-posedness, it is challenging for MSE-based models to address the color inconsistency issue. Thus, we adopt generative adversarial training to solve this problem.

In the initial version, we use a separate network consisting of a UNet with a soft mask for highlight region as the generator [3]. However, the improvement of visual quality is limited. Besides, this network introduces high computational costs. In this paper, we abandon the use of building an independent network for highlight generation. Instead, we directly utilize the combination of pre-trained AGCM and LE networks as the generator, as shown in Figure 4. Then, we aim to enhance the ability of the joint network through generative adversarial training. This design offers two distinct advantages. First, generative adversarial training essentially brings the distribution of the output closer to that of the ground-truth image. Since well-exposed regions have already been effectively processed in previous stages, the training will focus on improving color transition in highlight regions. Second, it does not incur additional computational costs, thereby enhancing the overall efficiency. The generator is denoted as:

$$I_H = Generator(I_S) = LE(AGCM(I_S)), \quad (19)$$

where $LE(\cdot)$ and $AGCM(\cdot)$ represent the pretrained LE and AGCM networks. We adopt the UNet-style network as the discriminator following [47] and optimize the GAN training based on Relativistic GAN [48]. The overall loss function

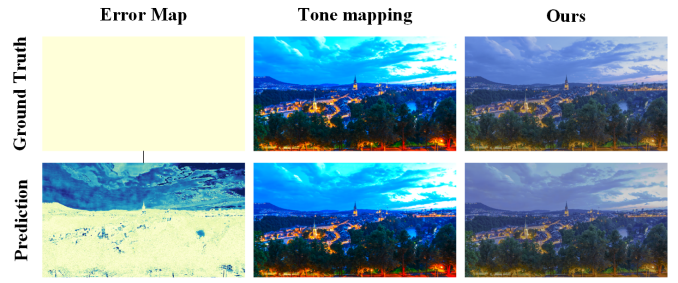


Fig. 5. Comparison of different visualization methods.

consists of three types of losses: L1 loss, perceptual loss [49] and GAN loss [50], [51], [52]. It can be formulated as:

$$L_{HR} = \lambda_1 L_1 + \lambda_2 L_{Percep} + \lambda_3 L_{GAN}, \quad (20)$$

where $\lambda_1, \lambda_2, \lambda_3$ are loss weights and we set them to 0.01, 1 and 0.005, respectively.

6 EXPERIMENTS

6.1 Experimental Setup

6.1.1 HDRTV1K dataset

Due to the limited availability of SDRTV/HDRTV data pairs for training and testing, we create an HDRTV dataset called HDRTV1K. This dataset includes 22 HDR videos (HDR10 standard) and their corresponding SDRTV versions sourced from YouTube, following [5]. All HDR videos are encoded using PQ-OETF in the Rec.2020 color gamut. We use 18 of 22 video pairs to generate image pairs for training, while the remaining 4 are set aside for testing. To minimize content similarity, we sample one frame every two seconds from each video, obtaining a training set of 1235 images. We also select 117 images extracted from the videos without repeated scenes to construct the test set.

6.1.2 Training details

For the proposed AGCM, the base network consists of 3 convolution layers with 1×1 kernel size and 64 channels, and the condition network contains 4 CCBs. Before training, we crop images by 480×480 with a step of 240. During training, patches of size 480×480 are input into the base network, while full images downsampled by a factor of 4 are input into the condition network. We set the mini-batch size to 4 and use the L1 loss function and Adam optimizer for training, with a total of 1×10^6 iterations. The initial learning rate is set to 4×10^{-4} , and is decayed by a factor of 2 at the 5×10^5 th iteration and 8×10^5 th iteration. For LE, we use the outputs of AGCM as the inputs. The mini-batch size is set to 8 and the patch size is 240×240 . The initial learning rate is set to 1×10^{-4} and is decayed by a factor of 2 after every 2×10^5 iterations, for a total of 1×10^6 iterations. L1 loss function and Adam optimizer are adopted for training. For joint training, the AGCM and LE networks are optimized simultaneously using the L1 loss function and Adam optimizer, with a batch size of 4 and the patch size of 192. The initial learning rate is set to 1×10^{-4} and is decayed by 2 after every 1×10^5 , for a total 5×10^5 iterations. We then train the GAN model with a batch size of 64 and a patch size

TABLE 1
Quantitative comparisons with existing methods.

Method		Params↓	PSNR↑	SSIM↑	SR-SIM↑	ΔE_{ITP} ↓	HDR-VDP3↑
LDR-to-HDR	HuoPhyEO [1]	-	25.90	0.9296	0.9881	38.06	7.893
	KovaleskiEO [6]	-	27.89	0.9273	0.9809	28.00	7.431
image-to-image translation	ResNet [53]	1.37M	37.32	0.9720	0.9950	9.02	8.391
	Pixel2Pixel [4]	11.38M	25.80	0.8777	0.9871	44.25	7.136
	CycleGAN [10]	11.38M	21.33	0.8496	0.9595	77.74	6.941
photo retouching	HDRNet [2]	482K	35.73	0.9664	0.9957	11.52	8.462
	CSRNet [14]	36K	35.04	0.9625	0.9955	14.28	8.400
	Ada-3DLUT [12]	594K	36.22	0.9658	0.9967	10.89	8.423
SDRTV-to-HDRTV	Deep SR-ITM [5]	2.87M	37.10	0.9686	0.9950	9.24	8.233
	JSI-GAN [13]	1.06M	37.01	0.9694	0.9928	9.36	8.169
	FMNet [18]	1.24M	37.94	0.9747	0.9957	8.10	8.51
HDRTVNet [3]	Base Network	5K	36.14	0.9643	0.9961	10.43	8.305
	AGCM	35K	36.88	0.9655	0.9964	9.78	8.464
	AGCM-LE	1.41M	37.61	0.9726	0.9967	8.89	8.613
	AGCM-LE-HG	37.20M	37.21	0.9699	0.9968	9.11	8.569
HDRTVNet++ (ours)	AGCM++	35K	37.35	0.9666	0.9968	9.29	8.511
	AGCM-LE++	591K	38.45	0.9739	0.9970	7.90	8.666
	AGCM-LE++†	591K	38.60	0.9745	0.9973	7.67	8.696
	AGCM-LE-HR++	591K	38.36	0.9735	0.9975	8.28	8.751

¹ Red, blue and green texts indicate the best, second best and third best results.

² † means the model is finetuned by joint training.

of 128. The initial learning rate is set to 1×10^{-4} and the total number of iterations is set to 4×10^5 . The learning rate is decayed by a factor of 0.5 at the 5×10^4 th, 1×10^5 th, 2×10^5 th and 3×10^5 th iteration. All models are built using PyTorch framework and trained with NVIDIA 3090 GPUs.

6.1.3 Evaluation

Metrics. We employ five evaluation metrics for comprehensive comparisons, including PSNR, SSIM, SR-SIM [15], HDR-VDP3 [17] and ΔE_{ITP} [16]. PSNR reflects the fidelity between SDRTV-to-HDRTV results and ground truth HDRTV images. SSIM and SR-SIM are used to measure image similarity. Although SR-SIM is designed to evaluate SDR images, [54] shows that SR-SIM also performs well for evaluating images in HDR standards. We additionally introduce ΔE_{ITP} to measure the color differences, as it is specifically designed for HDRTV content. HDR-VDP3 is an improved version of HDR-VDP2 that supports the Rec.2020 color gamut. For HDR-VDP3, results are compared by setting the “side-by-side” task, “rgb-bt.2020” color encoding, 50 pixels per degree, and “led-lcd-wcg” for the “rgb-display” option.

Visualization. We display HDRTV images in 16-bit “PNG” format without any additional processing. Since gamma EOTF is used to decode HDRTV images on SDR screens, they may appear relatively darker than that on HDR screens. However, visual differences can still be easily observed using our method. Previous work [5], [13] visualize HDRTV images using software (MPC-HC player). However, this comparison may be unfair, because video

players often introduce additional and unknown enhancement, especially for highlight regions of HDRTV content, resulting in similar visual results between the output and the ground truth. Another approach is to use error maps to show the intensity difference between the generated result and the corresponding ground truth. However, this method does not accurately reflect visual differences as perceived by humans. In contrast, our visualization method preserves details in highlight areas and presents visual differences that closely resemble human perception, as shown in Figure 5.

6.2 Comparison with Existing Methods

We compare our results with four types of methods: joint SR with SDRTV-to-HDRTV, image-to-image translation, photo retouching and LDR-to-HDR. Since these methods are not specifically designed for this task, we have made the necessary adjustment. For joint SR with SDRTV-to-HDRTV methods, we change the stride of the first convolutional layer to 2 for downsampling to match the size of the input and output.² For LDR-to-HDR methods, we process the results as illustrated in Figure 3(c). Note that we follow the same processing steps as [5], [13]. All data-driven methods are retrained on the proposed dataset.

Quantitative comparison. As shown in Table 1, our method significantly outperforms other methods on all evaluation metrics. Notably, our first step AGCM (the prili-

² We have also conducted experiments to remove the upsampling operation at the end of the networks instead of downsampling at the beginning, but results show that this do not improve performance and significantly increased computational cost in memory and runtime.

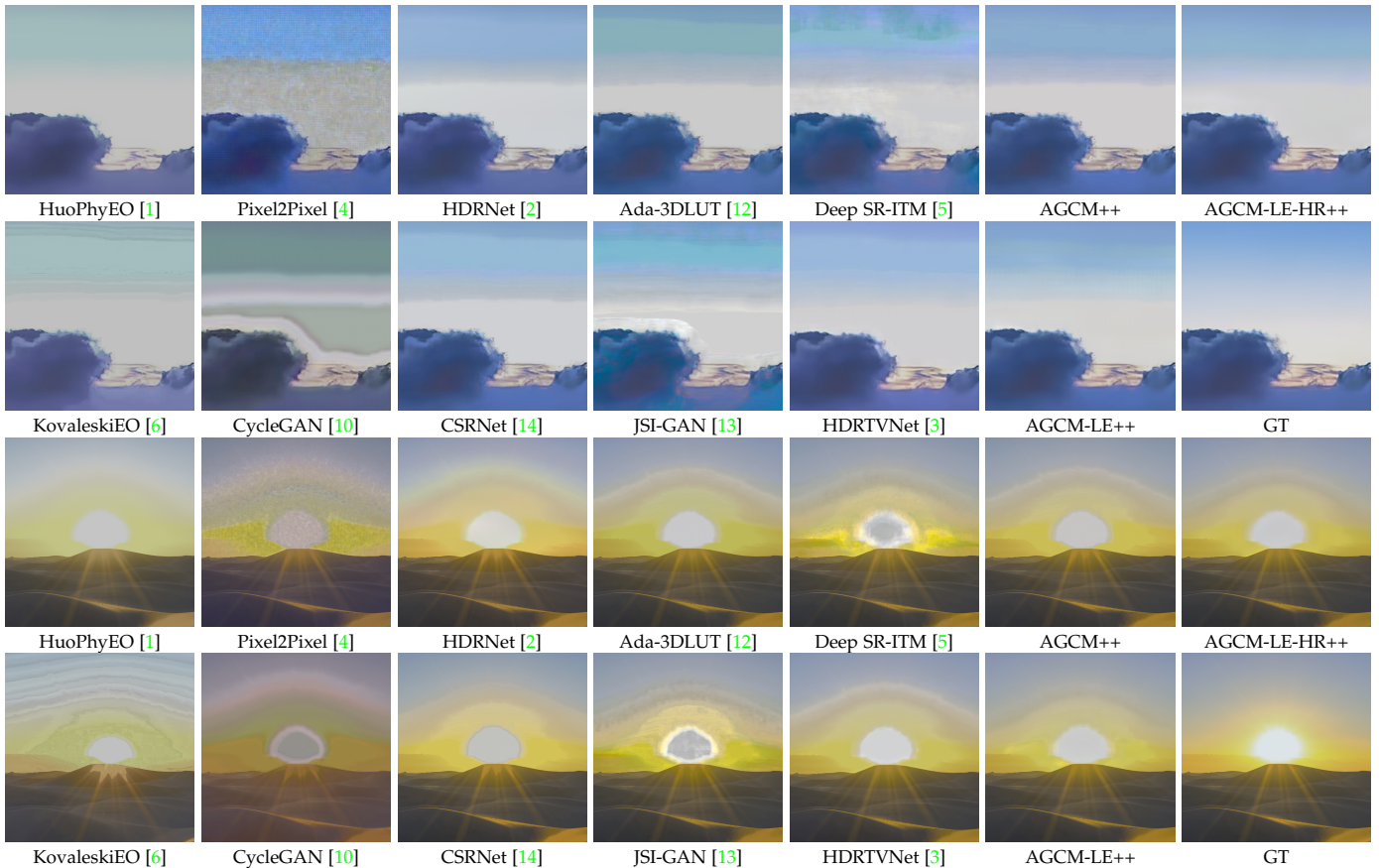


Fig. 6. Visual comparison on real dataset Urban of band 105.

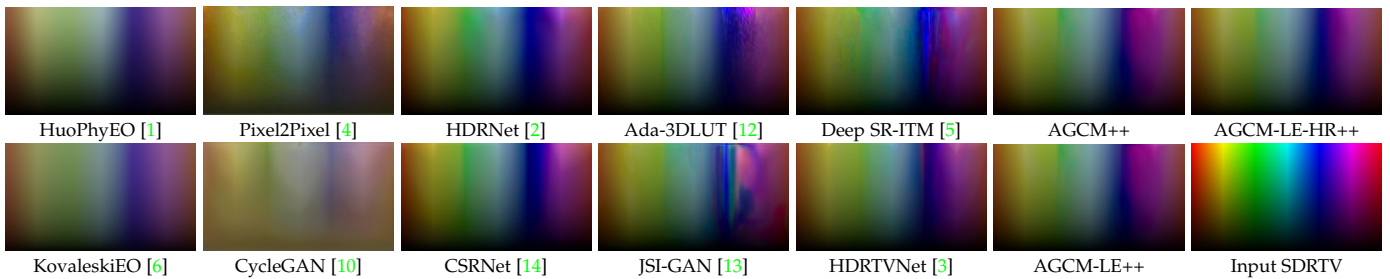


Fig. 7. Visual comparison on real dataset Urban of band 105.

inary version) already achieves comparable performance to Ada-3DLUT, but with only 1/17 of its parameters. By further optimizing the training of AGCM, the improved version, AGCM++, surpasses all compared methods except FMNet [18]. When equipped with the LE network and joint training, our method achieves 38.60dB and significantly outperforms all other approaches. Specifically, it obtains a performance gain of 0.66dB to the state-of-the-art method FMNet and achieves about 1dB compared to the preliminary version HDRTVNet. Equipped with the HR part, the generative adversarial training impairs PSNR performance, but achieves the best performance on HDR-VDP3 that measures perceptual quality. Moreover, it is noteworthy that our HDRTVNet++ is highly efficient and has significantly fewer parameters than other methods.

Visual comparison. Figure 6 shows the results of visual comparison. LDR-to-HDR-based and image-to-image translation methods tend to generate low-contrast images. Be-

sides, except for HuoPhyEO [1], LDR-to-HDR-based, image-to-image translation, and SDRTV-to-HDRTV approaches all produce unnatural colors and obvious artifacts. The results generated by photo retouching methods are relatively better but suffer from color cast. In contrast, our method produces natural colors and high contrast similar to the ground truth without additional artifacts. Moreover, the visual quality of results is improved by addition of processing steps, i.e., $AGCM < AGCM-LE < AGCM-LE-HR$. This also demonstrates the effectiveness of the overall solution pipeline.

6.3 Color Transition Test

We observe that many previous methods perform poorly in highlight regions, particularly where color changes occur. To reveal this phenomenon, we conduct a color transition test, as shown in Figure 7. We use a man-made color card as the input image, and compare the output results of different

TABLE 2
Quantitative comparisons between methods w/ and w/o AGCM.

Method	Params↓	PSNR↑	SSIM↑	SR-SIM↑	ΔE_{ITP} ↓	HDR-VDP3↑
LE(Basic3x3)	40K	36.98	0.9706	0.9989	9.63	8.368
AGCM-LE(Basic3x3)	75K	37.50	0.9721	0.9988	9.13	8.580
LE(ResNet)	1.37M	37.32	0.9720	0.9950	9.02	8.391
AGCM-LE(ResNet)	1.41M	37.61	0.9726	0.9967	8.89	8.613
LE(UNet)	556K	37.08	0.9705	0.9956	9.27	8.315
AGCM-LE(UNet)	591K	38.60	0.9745	0.9973	7.67	8.696

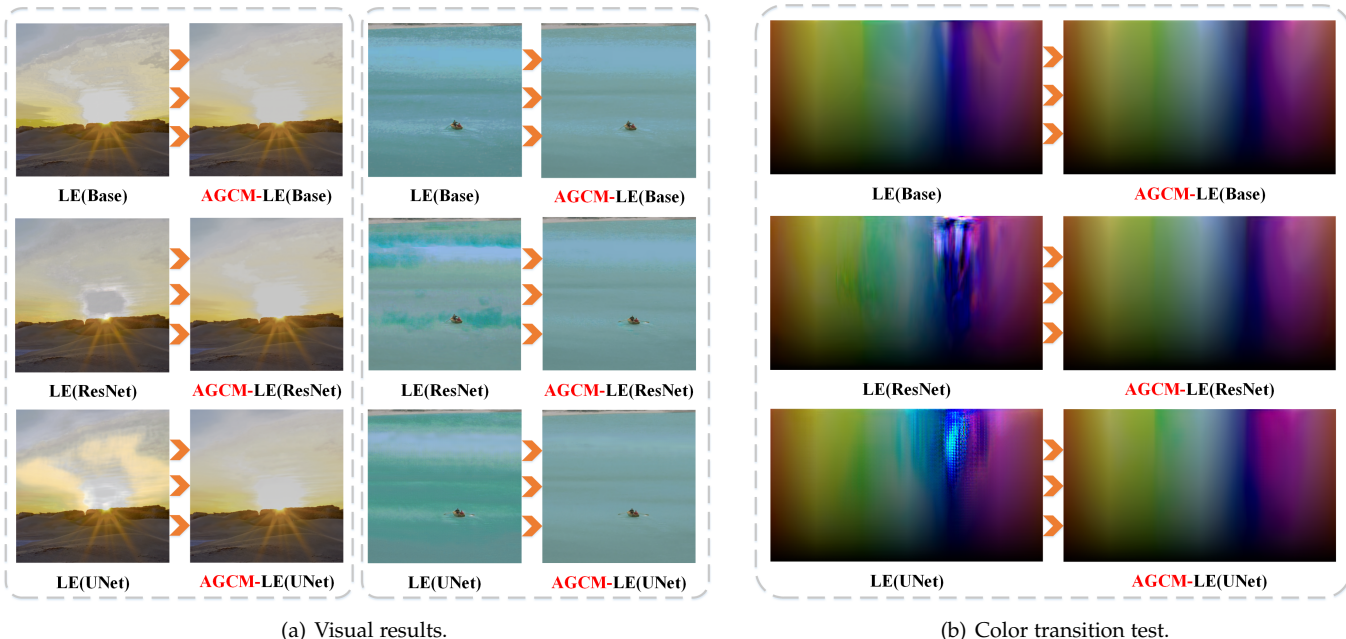


Fig. 8. Qualitative comparisons between methods w/ and w/o AGCM.

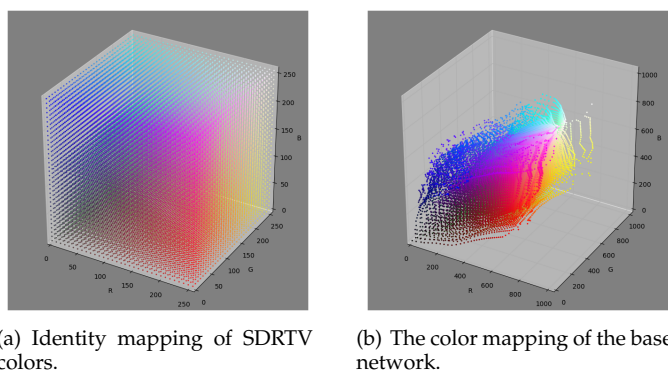


Fig. 9. Visualization of 3D LUTs.

methods. We can obtain several observations about this experiment. First, unnatural transitions and color blending problems appear in the outputs of methods that rely on region-dependent operations (e.g., Deep SR-ITM, JSI-GAN, Pixel2Pixel, CycleGAN) or the method that is based on conditions produced by region-dependent operations (i.e., 3D-LUT). In contrast, our method achieves smooth transition for AGCM that is based on pixel-independent operations. Moreover, when learning region-dependent mapping (e.g.,

AGCM-LE, AGCM-LE-HR), Our method also do not produce color transition artifacts. This demonstrates the superiority of our AGCM and the effectiveness of our cascaded solution pipeline. An interesting phenomenon is that blue regions suffer the most severe unnatural color transition. A reasonable explanation is that blue colors are more difficult to recover than other colors, because more information is lost in the blue area during color gamut compression.

6.4 Significance of AGCM

To demonstrate the necessity of AGCM, we conduct comprehensive experiments to show the quantitative and qualitative comparisons between methods with and without AGCM. In addition to using ResNet (used in the preliminary version) and UNet-based LE networks, we also implemented a very small-scale LE network, denoted as Basic3x3. It has the same architecture (i.e., three-layer convolution network) as our base network but replaces all 1x1 filters with 3x3 filters. As presented in Table 2, methods that perform AGCM before LE (i.e. AGCM+LE), with limited additional parameters, achieve significantly higher performance than methods that learn the LE network directly, regardless of the scale of the LE network. Additionally, Figure 8(a) shows that outputs from methods without AGCM exhibit

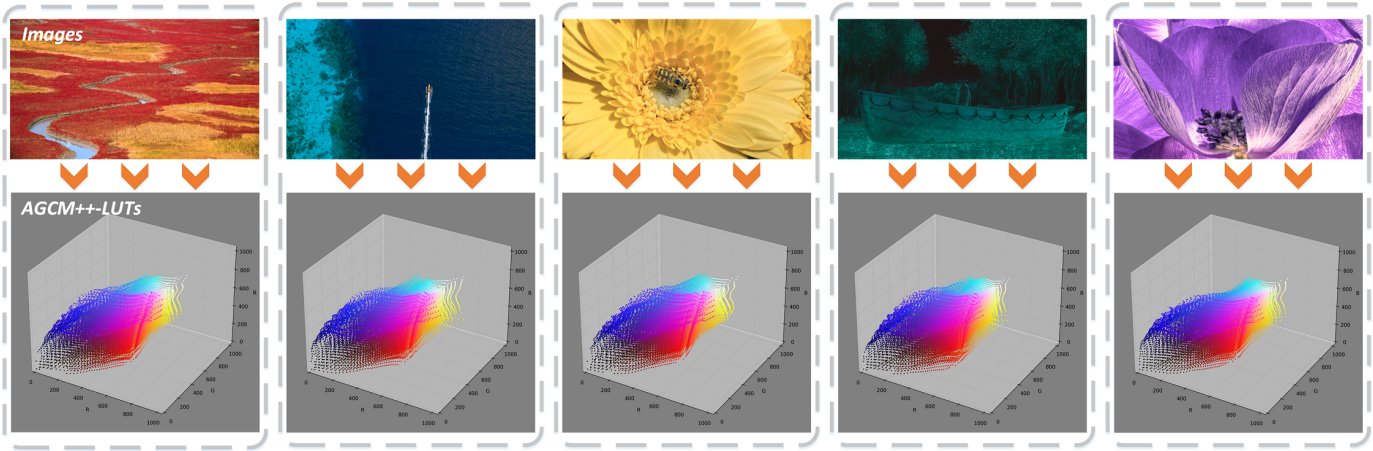


Fig. 10. 3D LUTs generated by taking various images as input conditions of our AGCM network.



Fig. 11. Visual results and 3D LUT manifolds in different stages.

noticeable artifacts in over-exposed and saturated regions. Figure 8(b) also demonstrates that methods without AGCM perform poorly in the color transition test. Besides, there is an interesting phenomenon that the larger the network scale, the more severe the artifacts. The smallest LE network Basic3x3 has the lowest performance but produce the best visual results. Both the quantitative and qualitative results indicate that performing AGCM prior to local enhancement is crucial for the final performance. We believe that this is because optimizing pixel-independent and region-dependent mapping together is challenging for an end-to-end LE network. Nevertheless, addressing color mapping before local enhancement can effectively and efficiently mitigate this optimization challenge and improve results.

6.5 Analysis of color mapping via LUT manifold

In this section, we present a comprehensive analysis of the function of our proposed model at various stages by visualizing the manifold of Look-Up Tables (LUTs). We begin by illustrating the LUT manifold and its visualization. In a 3D LUT cube, each point has four basic attributes: color and three coordinate values, which determine the position of the color within the current domain. Figure 9(a) shows the 3D LUT cube of the identity mapping of SDRTV colors, where the coordinate values of each point correspond to the three-channel values of its color in the SDRTV domain. For instance, the color (R:128, G:128, B:128) is located at the position (128, 128, 128) in the space. Figure 6.2 presents the LUT manifold of SDRTV-to-HDRTV color mapping using the base network. Within this cube, the coordinate values of each point correspond to its corresponding HDRTV color. It can be observed that SDRTV colors, ranging from 0 to 255, are mapped to HDRTV colors with a range of 0 to 1023. To demonstrate that our color condition can effectively achieve image-adaptive functionality, we show the manifold of different LUTs generated by our AGCM with various conditional inputs in Figure 10. As one can see that the LUT manifolds change according to different inputs, indicating the effectiveness of the color condition.

We further demonstrate the functionality of different steps using LUT manifold visualization in Figure 11. Firstly, the base network can only learn a one-to-one color mapping throughout the dataset, resulting in a non-smooth color transition of the LUT manifold in highlight areas and severe artifacts in the output. In contrast, the color condition network helps the base network learn image-adaptive color mapping, eliminating artifacts in the results generated by AGCM and densifying the LUT manifold. Secondly, due to local enhancement, the LUT manifold becomes more compact and smooth, allowing an SDRTV color to be mapped to multiple HDRTV colors through region-dependent operations (i.e., convolutions). It can handle one-to-many color mapping and greatly improve visual quality. Lastly, we can see that highlight refinement further compacts and densifies the LUT manifold, and the results also have natural color transition in highlight regions.

TABLE 3
Quantitative comparisons on the depth of the base network in AGCM.

Method	Params↓	PSNR↑	SSIM↑	SR-SIM↑	ΔE_{ITP} ↓	HDR-VDP3↑
AGCM-C5B2 ¹	30.2K	36.65	0.9664	0.9966	10.11	8.497
AGCM-C5B3	35.3K	37.35	0.9666	0.9968	9.29	8.511
AGCM-C5B4	40.3K	37.31	0.9662	0.9966	9.16	8.497
AGCM-C5B5	45.4K	37.31	0.9670	0.9969	9.35	8.504

¹ B means the depth of the base network, while C represents the depth of the condition network.

TABLE 4
Quantitative comparisons on the depth of the condition network in AGCM.

Method	Params↓	PSNR↑	SSIM↑	SR-SIM↑	ΔE_{ITP} ↓	HDR-VDP3↑
AGCM-C3B3 ¹	8.4K	36.42	0.9645	0.9966	10.25	8.492
AGCM-C4B3	13.9K	36.84	0.9667	0.9965	9.56	8.509
AGCM-C5B3	35.3K	37.35	0.9666	0.9968	9.29	8.511
AGCM-C6B3	118.8K	37.05	0.9663	0.9966	9.56	8.486

¹ B means the depth of the base network, while C represents the depth of the condition network.

TABLE 5
Quantitative comparisons on the critical layers in AGCM.

Method	Params↓	PSNR↑	SSIM↑	SR-SIM↑	ΔE_{ITP} ↓	HDR-VDP3↑
BaseModel-B3	4.6K	36.37	0.9556	0.9963	10.22	8.397
AGCM-woDropout ¹	35.3K	37.00	0.9658	0.9968	9.39	8.497
AGCM-woIN ²	34.8K	36.60	0.9645	0.9967	11.36	8.473
AGCM	35.3K	37.35	0.9666	0.9968	9.29	8.511

¹ *woDropout* means the Dropout layers are disabled.

² *woIN* indicates the Instance Normalization layers are disabled.

TABLE 6
Quantitative comparisons on different networks for LE.

Method	Params↓	PSNR↑	SSIM↑	SR-SIM↑	ΔE_{ITP} ↓	HDR-VDP3↑
LE ¹	1368K	38.32	0.9736	0.9971	8.14	8.635
LE++	556K	38.45	0.9739	0.9970	7.90	8.666

¹ LE denotes the network in our preliminary version [3] trained based on the same AGCM++ outputs.

6.6 Network Investigation

In this section, we conduct comprehensive experiments to investigate the specific network design.

Adaptive Global Color Mapping. We first examine the effects of the depths of the base network and the condition network in AGCM, as shown in Table 3 and Table 4. We vary the depth of the base network from 2 to 5, and find that the model with the depth of 3 achieves the best performance. We also set the depth of the condition network from 3 to 6, and the experiments demonstrate the condition network with a depth of 5 obtains better performance than others. Thus, in our final model, we set the depth of the base network and condition network to 3 and 5, respectively.

We also conduct an ablation study on the key components of the proposed AGCM. As presented in Figure 5, removing the Dropout layer from AGCM slightly reduces performance, indicating the effectiveness of Dropout in the condition network design. Notably, removing instance normalization will result in a significant performance drop. In this case, AGCM performs only slightly better than the base network without the condition. This illustrates that the instance normalization layer is critical for the effectiveness

of the proposed color condition. We believe it is because the operation of instance normalization can help the network learn some key attributions (i.e., contrast) as the condition.

Local Enhancement. In our preliminary version [3], we simply adopt a ResNet-style network to realize the local enhancement. Although the previous work has demonstrated its effectiveness, this part can be significantly improved to achieve better performance with higher efficiency. In this paper, we introduce a UNet-style network to perform local enhancement as described in Section 5.2. For fair comparison, we adopt the same AGCM model, i.e., AGCM++, prior to the LE network. As shown in Table 6, our LE++ obtains a large performance gain of more than 0.8dB compared to the previous LE with about only half of the parameters, indicating the superiority of LE++. There are two primary reasons for the success of our UNet-style LE network: (1) its U-shape design enables it to have stronger representational ability, particularly for high-resolution images; and (2) it is capable of handling spatially-variant mapping through the condition branch, making it especially suitable for operations that vary across different regions, such as local tone-mapping operators.

TABLE 7
Quantitative comparisons between the base network and its converted 3D LUTs.

Method	Params↓	PSNR↑	SSIM↑	SR-SIM↑	ΔE_{ITP} ↓	HDR-VDP3↑
Base network	5k	36.14	0.9643	0.9961	10.43	8.305
3DLUT_s33 ¹	108k	35.98	0.9645	0.9958	10.60	8.322
3DLUT_s64	786k	36.13	0.9643	0.9960	10.46	8.309

¹ The s33 or s64 represents the size of LUT. LUTs of these two sizes are commonly used in the process of production.

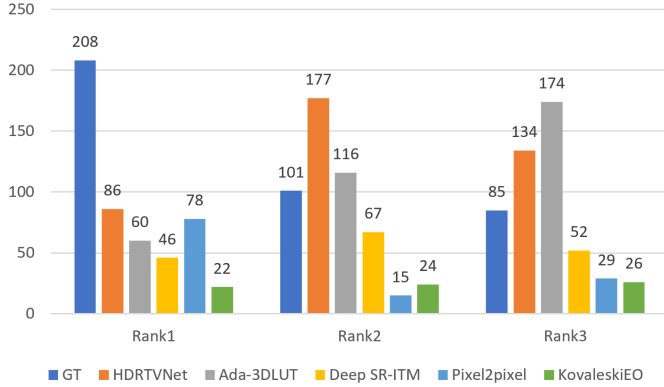


Fig. 12. User study rankings for different methods. Rank 1 means the best subjective feeling.

6.7 Conversion from base network to 3D LUT

3D Look-Up Tables (3D LUTs) are widely used in practical applications to manipulate the style and tone of images, particularly in the movie production chain as part of the digital intermediate process. Besides, there are many software and tools available for editing images by modifying 3D LUTs. Therefore, constructing the SDRTV-to-HDRTV 3D LUT is of great value for practical applications. The previous work [12] directly use 3D LUTs to build the photo retouching network. However, the 3D LUT network is not flexible for interpolation and modulation. To achieve image-adaptive functionality, multiple 3D LUTs need to be trained with a CNN weight predictor in [12]. In contrast, the base network in our method can be directly converted into a 3D LUT. Concretely, we take a 3D lattice composed of SDRTV colors as input and obtain the corresponding HDRTV colors. Then, we can build the lookup table according to these paired data. When performing color transformation, we can use lookup and trilinear interpolation operations as [12]. In Figure 7, we show that our base network can be converted to 3D LUTs with limited loss of accuracy. For a small size 3D LUT with 33 nodes (3DLUT_s33), the conversion causes a little performance drop with 0.16dB. Moreover, there is little performance loss when converting the network to a large 3D LUT (3DLUT_s64) with 64 nodes. In addition, our base network has only 5K parameters, so it is efficient for training. Note that the modulation is still can be performed on the base network to generate costumed 3D LUTs.

6.8 User Study

We first conduct a user study with 20 participants to subjectively evaluate the visual quality of HDRTVNet compared to four other methods with the best performance in each category. A total of 25 images are randomly selected from

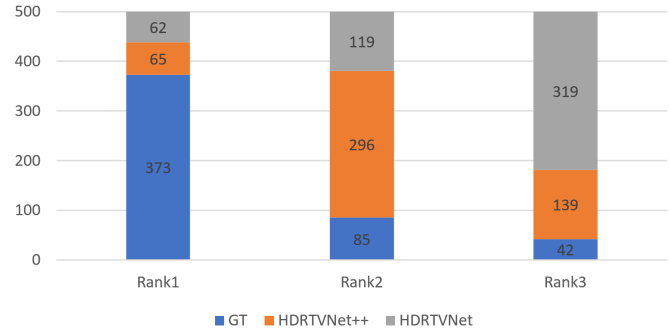


Fig. 13. User study rankings for HDRTVNet and HDRTVNet++. Rank 1 means the best subjective feeling.

the testing set and displayed on an HDR TV (Sony X9500G with a peak brightness of 1300 nits) in a darkroom. Before the experiment, we instruct the participants to consider three main factors when evaluating the images: (1) the presence of obvious artifacts and unnatural colors, (2) the naturalness and comfort of the overall color, brightness, and contrast, and (3) the perception of contrast between light and dark levels and highlight details. Based on these principles, participants rank the results of different methods in each scenario. The TV is set to the Rec.2020 color gamut and HDR10 standard when displaying the results.

We first compare five methods: Ada-3DLUT [12], Deep SR-ITM [5], Pixel2pixel [4], KovaleskiEO [6] and HDRTVNet [3], along with the ground-truth. When ranking the images for a scene, participants are able to view six images from different methods simultaneously or compare any two images at will until they decided on the order. We display the counts of different results in the top three ranks, as shown in Figure 12. The ground truth (GT) and our HDRTVNet account for 41.6% (208 counts) and 17.2% (86 counts) of the results considered to have the best visual quality, respectively. Similarly, HDRTVNet accounts for 35.4% of the results considered to have the second-best visual quality. In conclusion, the results of HDRTVNet are only inferior to the GT in terms of visual quality in subjective evaluation.

Furthermore, we conduct a user study to verify the superiority of the proposed HDRTVNet++ over the previous HDRTVNet [3]. Participants are asked to rank the images for each set in this user study with the same setup as the above. As shown in Figure 13, the ground-truth still achieve the best visual quality, while HDRTVNet++ shows a better ranking over HDRTVNet. HDRTVNet++ accounts for 59.2% (296 counts) of the results considered to have the second-best visual quality, which greatly outperforms HDRTVNet 23.8% (119 counts). All these results demonstrate the superiority of our method in terms of objective visual quality.

7 CONCLUSION

We have introduced a new SDRTV-to-HDRTV solution pipeline based on the SDRTV/HDRTV formation pipeline, using a divide-and-conquer approach. We have also introduced a new method, HDRTVNet++, to address this problem. Based on the different types of operations in the SDRTV/HDRTV formation pipeline, including pixel-independent and region-dependent operations, we propose implementing adaptive global color mapping and local enhancement separately. We have designed a new color condition network with fewer parameters and better performance than existing approaches to realize color mapping for SDRTV-to-HDRTV. To further enhance visual results, we have introduced generative adversarial training for highlight refinement. Additionally, we have constructed a new HDRTV dataset for training and testing. Comprehensive experiments demonstrate the superiority of our solution in terms of both quantitative comparison and visual quality.

REFERENCES

- [1] Y. Huo, F. Yang, L. Dong, and V. Brost, "Physiological inverse tone mapping based on retina response," *The Visual Computer*, vol. 30, no. 5, pp. 507–517, 2014. **1, 8, 9**
- [2] M. Gharbi, J. Chen, J. T. Barron, S. W. Hasinoff, and F. Durand, "Deep bilateral learning for real-time image enhancement," *ACM Transactions on Graphics (TOG)*, vol. 36, no. 4, pp. 1–12, 2017. **1, 2, 8, 9**
- [3] X. Chen, Z. Zhang, J. S. Ren, L. Tian, Y. Qiao, and C. Dong, "A new journey from sdrtv to hdrtv," in *Proceedings of the IEEE/CVF International Conference on Computer Vision*, 2021, pp. 4500–4509. **1, 2, 3, 5, 6, 7, 8, 9, 12, 13**
- [4] P. Isola, J.-Y. Zhu, T. Zhou, and A. A. Efros, "Image-to-image translation with conditional adversarial networks," in *Proceedings of the IEEE conference on computer vision and pattern recognition*, 2017, pp. 1125–1134. **1, 8, 9, 13**
- [5] S. Y. Kim, J. Oh, and M. Kim, "Deep sr-itm: Joint learning of super-resolution and inverse tone-mapping for 4k uhd hdr applications," in *Proceedings of the IEEE International Conference on Computer Vision*, 2019, pp. 3116–3125. **1, 2, 3, 5, 7, 8, 9, 13**
- [6] R. P. Kovaleski and M. M. Oliveira, "High-quality reverse tone mapping for a wide range of exposures," in *2014 27th SIBGRAPI Conference on Graphics, Patterns and Images*. IEEE, 2014, pp. 49–56. **1, 8, 9, 13**
- [7] B. Masia, S. Agustin, R. W. Fleming, O. Sorkine, and D. Gutierrez, "Evaluation of reverse tone mapping through varying exposure conditions," in *ACM SIGGRAPH Asia 2009 papers*, 2009, pp. 1–8. **1**
- [8] Y.-L. Liu, W.-S. Lai, Y.-S. Chen, Y.-L. Kao, M.-H. Yang, Y.-Y. Chuang, and J.-B. Huang, "Single-image hdr reconstruction by learning to reverse the camera pipeline," in *Proceedings of the IEEE/CVF Conference on Computer Vision and Pattern Recognition*, 2020, pp. 1651–1660. **1, 3, 4**
- [9] G. Eilertsen, J. Kronander, G. Denes, R. K. Mantiuk, and J. Unger, "Hdr image reconstruction from a single exposure using deep cnns," *ACM transactions on graphics (TOG)*, vol. 36, no. 6, pp. 1–15, 2017. **1**
- [10] J.-Y. Zhu, T. Park, P. Isola, and A. A. Efros, "Unpaired image-to-image translation using cycle-consistent adversarial networks," in *Proceedings of the IEEE international conference on computer vision*, 2017, pp. 2223–2232. **1, 8, 9**
- [11] Y. Liu, J. He, X. Chen, Z. Zhang, H. Zhao, C. Dong, and Y. Qiao, "Very lightweight photo retouching network with conditional sequential modulation," *IEEE Transactions on Multimedia*, 2022. **1, 5**
- [12] H. Zeng, J. Cai, L. Li, Z. Cao, and L. Zhang, "Learning image-adaptive 3d lookup tables for high performance photo enhancement in real-time," *IEEE Transactions on Pattern Analysis and Machine Intelligence*, vol. 44, no. 4, pp. 2058–2073, 2020. **1, 2, 8, 9, 13**
- [13] S. Y. Kim, J. Oh, and M. Kim, "Jsi-gan: Gan-based joint super-resolution and inverse tone-mapping with pixel-wise task-specific filters for uhd hdr video." in *AAAI*, 2020, pp. 11 287–11 295. **2, 3, 5, 8, 9**
- [14] J. He, Y. Liu, Y. Qiao, and C. Dong, "Conditional sequential modulation for efficient global image retouching," in *Computer Vision—ECCV 2020: 16th European Conference, Glasgow, UK, August 23–28, 2020, Proceedings, Part XIII 16*. Springer, 2020, pp. 679–695. **2, 5, 6, 8, 9**
- [15] L. Zhang and H. Li, "Sr-sim: A fast and high performance iqa index based on spectral residual," in *2012 19th IEEE international conference on image processing*. IEEE, 2012, pp. 1473–1476. **2, 8**
- [16] ITU-R, "Objective metric for the assessment of the potential visibility of colour differences in television," ITU-R Rec, BT.2124-0, Tech. Rep., 2019. **2, 8**
- [17] R. Mantiuk, K. J. Kim, A. G. Rempel, and W. Heidrich, "Hdr-vdp-2: A calibrated visual metric for visibility and quality predictions in all luminance conditions," *ACM Transactions on graphics (TOG)*, vol. 30, no. 4, pp. 1–14, 2011. **2, 8**
- [18] G. Xu, Q. Hou, L. Zhang, and M.-M. Cheng, "Fmnet: Frequency-aware modulation network for sdr-to-hdr translation," in *Proceedings of the 30th ACM International Conference on Multimedia*, 2022, pp. 6425–6435. **2, 3, 5, 8, 9**
- [19] G. He, K. Xu, L. Xu, C. Wu, M. Sun, X. Wen, and Y.-W. Tai, "Sdrtv-to-hdrtv via hierarchical dynamic context feature mapping," in *Proceedings of the 30th ACM International Conference on Multimedia*, 2022, pp. 2890–2898. **2, 3**
- [20] Z. Cheng, T. Wang, Y. Li, F. Song, C. Chen, and Z. Xiong, "Towards real-world hdrtv reconstruction: A data synthesis-based approach," in *Computer Vision—ECCV 2022: 17th European Conference, Tel Aviv, Israel, October 23–27, 2022, Proceedings, Part XIX*. Springer, 2022, pp. 199–216. **2, 3**
- [21] M. Yao, D. He, X. Li, Z. Pan, and Z. Xiong, "Bidirectional translation between uhd-hdr and hd-sdr videos," *IEEE Transactions on Multimedia*, 2023. **2**
- [22] C. Guo, L. Fan, Z. Xue, and X. Jiang, "Learning a practical sdr-to-hdrtv up-conversion using new dataset and degradation models," in *Proceedings of the IEEE/CVF Conference on Computer Vision and Pattern Recognition*, 2023, pp. 22 231–22 241. **2, 3**
- [23] ITU-R, "Parameter values for the hdtv standards for production and international programme exchange," ITU-R Rec, BT.709-6, Tech. Rep., 2015. **2, 4**
- [24] ITU-R, "Reference electro-optical transfer function for flat panel displays used in hdtv studio production," ITU-R Rec, BT.1886, Tech. Rep., 2011. **2**
- [25] ITU-R, "Parameter values for ultra-high definition television systems for production and international programme exchange," ITU-R Rec, BT.2020-2, Tech. Rep., 2015. **2, 4**
- [26] ITU-R, "Image parameter values for high dynamic range television for use in production and international programme exchange," ITU-R Rec, BT.2100-2, Tech. Rep., 2018. **2, 4**
- [27] S. Y. Kim, D.-E. Kim, and M. Kim, "Itm-cnn: Learning the inverse tone mapping from low dynamic range video to high dynamic range displays using convolutional neural networks," in *Computer Vision—ACCV 2018: 14th Asian Conference on Computer Vision, Perth, Australia, December 2–6, 2018, Revised Selected Papers, Part III 14*. Springer, 2019, pp. 395–409. **3**
- [28] ITU-R, "Colour conversion from recommendation itu-r bt.709 to recommendation itu-r bt.2020," ITU-R Rec, BT.2087-0, Tech. Rep., 2015. **3, 4**
- [29] S. W. Zamir, J. Vazquez-Corral, M. Bertalmio *et al.*, "Gamut mapping in cinematography through perceptually-based contrast modification," *IEEE Journal of Selected Topics in Signal Processing*, vol. 8, no. 3, pp. 490–503, 2014. **3**
- [30] S. W. Zamir, J. Vazquez-Corral, and M. Bertalmio, "Gamut extension for cinema: psychophysical evaluation of the state of the art and a new algorithm," *Human Vision and Electronic Imaging XX*, vol. 9394, pp. 278–289, 2015. **3**
- [31] F. Schweiger, T. Borer, and M. Pindoria, "Luminance-preserving color conversion," *SMPTE Motion Imaging Journal*, vol. 126, no. 3, pp. 45–49, 2017. **3**
- [32] S. W. Zamir, J. Vazquez-Corral, and M. Bertalmio, "Gamut extension for cinema," *IEEE Transactions on Image Processing*, vol. 26, no. 4, pp. 1595–1606, 2017. **3**
- [33] L. Xu, B. Zhao, and M. R. Luo, "Color gamut mapping between small and large color gamuts: part ii. gamut extension," *Optics Express*, vol. 26, no. 13, pp. 17 335–17 349, 2018. **3**
- [34] S. W. Zamir, J. Vazquez-Corral, and M. Bertalmio, "Vision models for wide color gamut imaging in cinema," *IEEE Transactions on Pattern Analysis and Machine Intelligence*, vol. 43, no. 5, pp. 1777–1790, 2019. **3**

- [35] ITU-R, “High dynamic range television for production and international programme exchange,” ITU-R Rec, BT.2390-8, Tech. Rep., 2020. [3](#)
- [36] F. Drago, K. Myszkowski, T. Annen, and N. Chiba, “Adaptive logarithmic mapping for displaying high contrast scenes,” in *Computer graphics forum*, vol. 22, no. 3. Wiley Online Library, 2003, pp. 419–426. [3](#)
- [37] E. Reinhard, “Parameter estimation for photographic tone reproduction,” *Journal of graphics tools*, vol. 7, no. 1, pp. 45–51, 2002. [3](#)
- [38] J. Tumblin and H. Rushmeier, “Tone reproduction for realistic images,” *IEEE Computer graphics and Applications*, vol. 13, no. 6, pp. 42–48, 1993. [3](#)
- [39] G. W. Larson, H. Rushmeier, and C. Piatko, “A visibility matching tone reproduction operator for high dynamic range scenes,” *IEEE Transactions on Visualization and Computer Graphics*, vol. 3, no. 4, pp. 291–306, 1997. [3](#)
- [40] D. Lischinski, Z. Farbman, M. Uyttendaele, and R. Szeliski, “Interactive local adjustment of tonal values,” *ACM Transactions on Graphics (TOG)*, vol. 25, no. 3, pp. 646–653, 2006. [3](#)
- [41] J. Hable, “Uncharted 2: Hdr lighting,” in *Game Developers Conference*, 2010, p. 56. [4](#)
- [42] SMPTE, “High dynamic range electro-optical transfer function of mastering reference displays,” SMPTE, SMPTE ST2084:2014, Tech. Rep., 2014. [4](#)
- [43] X. Wang, K. Yu, C. Dong, and C. Change Loy, “Recovering realistic texture in image super-resolution by deep spatial feature transform,” in *Proceedings of the IEEE conference on computer vision and pattern recognition*, 2018, pp. 606–615. [5](#), [7](#)
- [44] X. Chen, Y. Liu, Z. Zhang, Y. Qiao, and C. Dong, “Hdrrunet: Single image hdr reconstruction with denoising and dequantization,” in *Proceedings of the IEEE/CVF Conference on Computer Vision and Pattern Recognition*, 2021, pp. 354–363. [5](#), [6](#)
- [45] V. Dumoulin, J. Shlens, and M. Kudlur, “A learned representation for artistic style,” in *International Conference on Learning Representations*, 2016. [6](#)
- [46] W. Shi, J. Caballero, F. Huszár, J. Totz, A. P. Aitken, R. Bishop, D. Rueckert, and Z. Wang, “Real-time single image and video super-resolution using an efficient sub-pixel convolutional neural network,” in *Proceedings of the IEEE conference on computer vision and pattern recognition*, 2016, pp. 1874–1883. [6](#)
- [47] X. Wang, L. Xie, C. Dong, and Y. Shan, “Real-esrgan: Training real-world blind super-resolution with pure synthetic data,” in *Proceedings of the IEEE/CVF International Conference on Computer Vision*, 2021, pp. 1905–1914. [7](#)
- [48] A. Jolicoeur-Martineau, “The relativistic discriminator: a key element missing from standard gan,” in *International Conference on Learning Representations*, 2018. [7](#)
- [49] J. Johnson, A. Alahi, and L. Fei-Fei, “Perceptual losses for real-time style transfer and super-resolution,” in *Computer Vision—ECCV 2016: 14th European Conference, Amsterdam, The Netherlands, October 11–14, 2016, Proceedings, Part II 14*. Springer, 2016, pp. 694–711. [7](#)
- [50] I. Goodfellow, J. Pouget-Abadie, M. Mirza, B. Xu, D. Warde-Farley, S. Ozair, A. Courville, and Y. Bengio, “Generative adversarial nets,” in *Advances in neural information processing systems*, 2014, pp. 2672–2680. [7](#)
- [51] Y. Blau and T. Michaeli, “The perception-distortion tradeoff,” in *Proceedings of the IEEE conference on computer vision and pattern recognition*, 2018, pp. 6228–6237. [7](#)
- [52] C. Ledig, L. Theis, F. Huszár, J. Caballero, A. Cunningham, A. Acosta, A. Aitken, A. Tejani, J. Totz, Z. Wang *et al.*, “Photo-realistic single image super-resolution using a generative adversarial network,” in *Proceedings of the IEEE conference on computer vision and pattern recognition*, 2017, pp. 4681–4690. [7](#)
- [53] K. He, X. Zhang, S. Ren, and J. Sun, “Identity mappings in deep residual networks,” in *European conference on computer vision*. Springer, 2016, pp. 630–645. [8](#)
- [54] S. Athar, T. Costa, K. Zeng, and Z. Wang, “Perceptual quality assessment of uhd-hdr-wcg videos,” in *2019 IEEE International Conference on Image Processing (ICIP)*. IEEE, 2019, pp. 1740–1744. [8](#)